Environmental Pollution 387 (2025) 127304

Contents lists available at ScienceDirect

Environmental Pollution

journal homepage: www.elsevier.com/locate/envpol

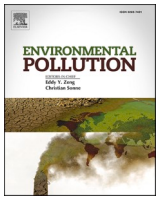

Labile fraction-based assessment of rare earth elements in contaminated sediments☆

María Dolores Basallote [a,*], Aarón Méndez [b], Rafael León [b], Manuel Olías [b], Rémi Freydier [c], Rafael Pérez-López [b], Carlos Ruiz Cánovas [b]

[a] Institute of Marine Sciences of Andalusia (ICMAN), Spanish National Research Council (CSIC), Department of Ecology and Coastal Management, E-11510, Puerto Real, Spain
[b] Department of Earth Sciences & Research Center on Natural Resources, Health and the Environment, University of Huelva, Campus "El Carmen", E-21071, Huelva, Spain
[c] HydroSciences Montpellier (HSM), Université de Montpellier, CNRS, IRD, Montpellier, France

ARTICLE INFO

Keywords:
Passive samplers
Lanthanides
Bioavailability
Acid mine drainage
Coastal pollution

ABSTRACT

The distribution and bioavailability of lanthanides in metal-rich sediments have been studied performing a transect sampling across an estuary affected by acid mine drainage and the combination of 24 h passive sampler deployment (diffusive gradient in thin films; DGTs) and determination of labile fractions (i.e., porewaters, acid-extractable, associated to carbonate and ion-exchangeable). Relationship between concentrations in DGTs and the rest of labile fractions were no observable. Rare earth elements (REE) in DGTs ranged from 0.75 to 4.9 μg L^{-1}, while in porewaters most samples exhibited values below the detection limit of the equipment, which highlights the suitability of these devices to monitor trace pollutants at low concentrations in estuarine sediments. A spatial trend in REE and Y absorption by DGT was observed, with increasing values with river influence. REE and Y are preferentially associated to the carbonate-associated and acid-extractable fractions, although exhibiting a high variability (3.7–74 % for REE and 6.4–94 % for Y in the acid-extractable fraction and from 1.0 to 71 % for REE and 2.0–95 % for Y in the carbonate-associated fraction) but scarcely contained in the ion-exchangeable fraction. This variability seems to be controlled by the mineralogical assemblage, especially those REE-carrying minerals such as Al oxyhydrosulfates, phosphates, Fe oxyhydroxysulfates and aluminosilicates. REE and Y appears to be preferentially associated to Al and S in the acid-extractable fraction while in the carbonate-associated one these elements seem to be related to Fe and P. The application of NASC-normalized patterns to environmental compartments suggests REE and Y retained in the sediment not only come from labile species in porewaters but also from the passing of Al nanoparticles and colloids through the diffusion layers of the DGTs. This information would have important implications for the validation of these devices for monitoring REE and Y exposure in heavily metal-polluted sediments worldwide.

1. Introduction

Technology metals (TMs) are increasingly used in high-tech applications such as telecommunications technology, the manufacturing of semiconductors, electronic displays and optical and energy-related devices (Eggert, 2011). Among them, rare earth elements (REE) stand out due to their economic importance and increasing emissions to the environment. Although REE are traditionally separated into two groups; light rare earth elements (LREE from La to Eu) and heavy rare earth elements (HREE, from Gd to Lu) (IUPAC et al., 2005), recent classifications divide them into three different groups: LREE (from La to Pm), medium REE (MREE, from Sm to Gd) and HREE (from Tb to Lu). Because analogous chemical properties related to their electronic configuration, which makes them almost inseparables during analytical determinations or even commercial extraction, scandium and yttrium are also considered within the REE group. REE in the environment come mainly from geogenic sources, but their contribution from high-tech devices and other sources such as industrial, agriculture and medicine is growing

☆ This paper has been recommended for acceptance by Dr Hefa Cheng.

* Corresponding author.
E-mail address: mdolores.basallote@csic.es (M.D. Basallote).

https://doi.org/10.1016/j.envpol.2025.127304
Received 18 August 2025; Received in revised form 3 October 2025; Accepted 20 October 2025
Available online 22 October 2025

interruptedly in the last years (Arienzo et al., 2022). These increasing emissions of REE have led to increasing concentration in waters and sediments, especially in estuaries and coastal areas (Brito et al., 2018; Delgado et al., 2012; Neira et al., 2022), posing a significant potential for increasing exposure to living organisms. Discharge from rivers, sewage and industrial effluents in estuaries constitutes a huge environmental quandary, especially for those TMs that have suffered a drastic increase in emissions such as La and Nd (Geagea et al., 2007). In addition, the fractionation of these elements in environmental matrices offers critical insights into the basic physicochemical processes governing their distribution and behavior (Chakhmouradian and Wall, 2012). For all these reasons, REE distribution in estuarine sediments as well as their exposure to benthic organisms should be monitored as part as programs assessing environmental status.

Diffusive gradient in thin-films (DGTs) are increasingly considered as an alternative technique to study REE and Y (REY) exposure in aquatic organisms. Providing simple, reliable, and sensitive measurements of DGT-labile metal species (e.g., free ions, inorganic form and metal weakly bonded to organic ligands), these passive samplers allow testing potentially toxic elements (PTE) bioavailability, as it has been pointed out at DGT-labile metal concentrations as the fraction that best predicts toxicity to exposed organisms (Amato et al., 2016; Cindrić et al., 2020; Davison, 2016; Menegário et al., 2017; Philipps et al., 2019). The use of DGT passive samplers as a complementary tool for discrete sampling has been reported for about 20 years, showing a good performance to monitor metal availability in aquatic environments (Cánovas et al., 2020a; Cánovas et al., 2020b; Gao et al., 2019; Marrugo-Madrid et al., 2021). Recently, the researcher community (e.g., Amouroux et al., 2023, Miège et al., 2015) proposes the use of DGT in a regulatory context at European level (e.g., to set up frequency and period of deployment for DGTs), in the structure of the Water Framework Directive (WFD; Directive, 2000/60/EC) by defining a standard guideline for using DGTs.

While metal bioaccesibility and toxicity in sediments have been previously approached using DGT (Amato et al., 2014, 2016; 2018; Gillmore et al., 2021), its application to study REY exposure has been scarcely documented in estuarine sediments. For instance, the amount of trace elements that can be released from the contaminated sediments to the water column in the Belgian coast has been estimated in the range of 4.4×10^{-5} to 0.10 mmol m^{-2} d^{-1} for Co, Pb, Cr, As, Cu, Ni, Fe, and Mn using DGT devices (Gao et al., 2009). The first laboratory ecotoxicological assessment of REE in intertidal sediments of the Pearl River estuary (China) using DGTs showed a low toxicological risk for benthic organisms (Gu et al., 2020). However, these studies need to be extended to other estuaries affected by anthropogenic contamination. In this sense, a remarkable example of metal pollution is the Ria of Huelva estuary (SW Spain), historically affected by mining and industrial activities. This estuary receives huge loads of inorganic pollutants from the Tinto and Odiel rivers (Nieto et al., 2007), among them REE. For instance, only the Tinto River delivers around 5.8 ton/yr of dissolved REE (Cánovas et al., 2021) to the estuary, which are chiefly trapped in the sediments during the estuarine mixing processes of acidic waters (pH ~ 3.0) and alkaline seawater (Borrego et al., 2004; Pérez-López et al., 2023). In addition, around 144 kg/yr of REY are released from a nearby phosphogypsum stack deposited in the estuarine marshlands since the 60s (Cánovas et al., 2018). These REY fluxes from mining as well as those from industrial origin (i.e., petrochemical industry, Cu smelter or former paper mills), also located in the estuary, may be added to those related to agricultural, medical and mass consumption goods in the area, with a total population of around 350,000 inhabitants. Definitely, the Ria of Huelva is an ultimate setting worldwide to study the bioavailability of REY in polluted estuarine sediments. Hence, the main goals of this work are: i) to study the REY distribution in estuarine sediments of the Ria of Huelva, ii) to determine the labile fractions of REY in the sediments studied, iii) determining the REY bioaccessibility using DGT devices, and iv) identifying the factors controlling the bioavailability of REY in such polluted sediments.

2. Study area

The Ria of Huelva estuary is formed by the confluence of the acidic Tinto and Odiel rivers with seawater (Supporting information; Fig. S1). This work focuses on the Odiel estuary because of its exceptional ecological status (UNESCO Biosphere Reserve, Ramsar site), which is intensively affected by acid mine drainage (AMD) as a result of a long history of mining in more than 80 sulfide mines distributed across the Odiel river watershed. The water depth decreases progressively from the upper to the lower part of the estuary, with maximum depths of 13 m (Cánovas et al., 2020a). This semidiurnal mesotidal regime estuary (mean tidal range of 2.69 m) is characterized by two different mixing processes, a pH-induced water mixture in the upper part of the estuary, and a salt-induced mixing in the lower one (Borrego et al., 2004). Thus, these mixing processes between the volume of acidic river waters and the neutral seawater predominantly control the hydrochemical properties of the Odiel estuary. During the mixture, intense removal of metals (e.g., Fe, Al, or Cu) from the water column takes place due to the progressive rise in pH values, leading to the enrichment in metals of estuarine sediments (Besada et al., 2022; López-González et al., 2006; Pérez-López et al., 2023; Ruiz et al., 2020). Besides the long-lasting mining chronic contamination, the estuary has also been affected by industrial pollution because of the settlement of an industrial complex in the 60's of the last century, composed mainly of a pyrite roasting and copper smelting plant, a paper mill, a fertilizer factory (which has generated extensive stacks of phosphogypsum), and a petrochemical complex (Sainz et al., 2004).

3. Methodology

3.1. Sediment and porewater sampling

A sampling was performed along the Odiel estuary to reflect the hydrochemical gradients observed in the estuary, selecting tidally-flooded sampling sites according to the river influence and the proximity to pollution sources (Fig. S1). With the higher river influence, sampling point OS1 is located close to a small urban settlement. OS2 is located downstream, near an abandoned mineral processing plant, where large waste dumps were placed and estuarine soils evidence a high degree of pollution (e.g., up to 9.8 g kg^{-1} of Pb, 1.5 g $kg^{-1}$of As, 1.5 g kg^{-1} of Zn, and 705 mg kg^{-1} of Cu; Grantcharova and Fernández--Caliani, 2021). OS3 and OS4 sampling points correspond to transitional environments from river to seawater with abundance of halophyte plants (*Salicornia* and *Spartina* spp.), and included in a Biosphere Reserve declared by UNESCO since 1983. Finally, OS5 has the largest seawater influence, located in the outer part of the estuary, at the entrance of the Padre Santo channel where ships enter to port, and near the chemical industrial complex (Fig. S1).

Sediment were collected at tidally influenced sites in the estuarine margin channel introducing PVC tubes 15 cm deep, adjacent to DGT devices (see section 3.2). The cores were sealed, preserved in refrigerated conditions, and transported to the laboratory at the University of Huelva (Spain), where they were sliced in 3 cm layers. About 30 mL sediment subsamples were frozen at −20 °C in sterile plastic bags and freeze-dried (Telstar LyoQuest, −40 °C and 0.2 mbar of pressure) before analysis. Other aliquots of each sediment layer were used to obtain porewaters, centrifuging at 3500 rpm during 5 min. Porewater solutions (20 mL) were immediately filtered through 0.45 μm pore size Millipore filters, stored in high-density polyethylene (HDPE) vials, acidified to pH < 2 with nitric acid 69 % Merck Suprapur®, and preserved in a refrigerator until analysis. Subsequently, physicochemical parameters such as temperature, pH, oxidation-reduction potential (ORP), and electrical conductivity (EC) were immediately measured in the remaining water using HANNA HI 98190 and 98192 portable meters. A three-point

calibration was performed for both EC (147 μS/cm, 1413 μS/cm, and 12.88 mS/cm) and pH (4.01, 7.00, and 9.21), while the ORP was controlled using two points (240 and 470 mV). For OS5 was not possible to obtain enough amount of porewaters from the deeper layers due to their high sand content.

3.2. DGT device settings

Sediment DGT passive samplers (LSPX-NP Loaded DGT device DGT® Research), which accumulate the labile fraction of metals showing affinity to a Chelex resin, were sunk (approximately 15 cm) in the sediment at the selected sampling sites, with the exposure window at the sediment-water interface, following the instructions given by the distributor. These passive samplers are designed to allow the diffusion of free cations and labile metal complexes (labile fraction) through a polyethersulphone filter membrane (0.45 μm porosity) and a 0.8 mm APA diffusive gel due to a concentration gradient, being accumulated in a mixed binding layer of Chelex and titanium oxide (Metsorb), the Chelex-100 resin gel. Having a dimension of 5 × 240 × 40 mm and an exposure window of 18 × 150 mm, the LSPX-NP DGT device has been especially designed to measure up to 40 metals (Panther et al., 2014). After about 24 h of exposure, the DGT devices were successively retrieved from the sediments, generously rinsed with Milli-Q water, kept in cold conditions, and transported in sterile plastic bags to the laboratory. Subsequently, the devices were dismantled, each gel resin was sliced in 3 cm segments, which were placed in separated acid washed polyethylene vials containing 1 mL ultrapure HNO_3 (1 M), and shaken at 60 rpm for 24 h (Ardelan et al., 2009; Basallote et al., 2020). Finally, the elution extracts were diluted with Milli-Q water to 10 mL prior to metal determination. Element concentrations in the DGT devices were determined according to the equations Eq (1) and Eq (2):

$$C_{DGT} = \frac{M^* \Delta g}{D^* A^* t} \quad \text{Eq (1)}$$

$$M = \frac{Ce\,(Vgel + Ve)}{fe} \quad \text{Eq (2)}$$

where C_{DGT} is the concentration of metal in the bulk solution measured by the DGT device, M is the mass of metal accumulated in the binding layer (ng), Δg is the thickness of the diffusive gel (0.078 cm) plus the thickness of the filter membrane used (0.014 cm), D is the diffusion coefficient of each metal ($cm^2\ s^{-1}$), A is the DGT cross-sectional exposure area (5.4 cm^2), and t is the deployment time in s (exact time for each exposure period), Ce is the concentration of element in the eluent (μg L^{-1}), $Vgel$ and Ve are the volumes (mL) of the gel and eluent, respectively, and fe is the elution factor. The diffusion coefficients (D) used for REE and Y were those reported by Yuan et al. (2018).

3.3. Sequential extractions

To study the metal bioavailability in collected sediments, long-established approaches such as sequential extraction schemes were also performed. The first extraction procedure to obtain the acid-extractable metal fraction was done using a 0.11 M acetic acid (CH_3-COOH) solution. Following the method from Rosado et al. (2015), 1 g of sediment was put into contact with 40 mL of solution, with continuous shaking, during 16 h. Afterwards, the sample was centrifuged and the supernatant was filtered, acidified and preserved until analysis. The second extraction is a modification of the Tessier sequential extraction, where the metal exchangeable fraction was determined after contacting 3 g of sediment with 24 mL of 1 M $MgCl_2$ solution at pH 7 during 1 h. This fraction represents the metal pool weakly adsorbed to sediments. After centrifugation (15 min at 3000 rpm), samples were filtered, acidified and preserved until analysis. Thereafter, the solids washed with Milli-Q water to remove the residue of $MgCl_2$ solution were put into contact with 24 mL of a 1 M sodium acetate (CH_3-COONa) solution at pH 5 for 5 h. Finally, samples were centrifuged, filtered, acidified and preserved until analysis to obtain the fraction representing the associated to carbonates metal pool. For the total digestion, 100 mg of sediments were put into contact with 4.5 mL of HNO_3, 1 mL of HCl and 1 mL of HF, and heated progressively up to 200 °C in 20 min (5 min at 100 °C, 5 min at 150 °C and 10 min at 200 °C) using a pressurized (40 bars) microwave Ultrawave (Milestone®). The solution was then transferred into Savillex vials and heated at 80 °C until total evaporation. The solid residue was recovered using 10 % HNO_3 and diluted with ultrapure water for chemical determination.

3.4. Analytical determinations

Trace metal(loid) determination in DGT and sediments elution extracts were performed by iCAP TQ ICP-MS (Thermo Scientific ®) at the AETE-ISO Platform (OSU OREME, Université de Montpellier, France). Trace concentrations in porewaters were determined without any prior dilution, using Kinetic Energy Discrimination - Argon Gas Dilution (KED-AGD mode). For all trace element determinations, an internal solution containing Be, Sc, Ge, Rh, and Ir was added on-line to the samples to correct signal drifts. Control reference materials for trace metals (CASS-6 and SLRS-6, PACS-3) were also analyzed to check the analytical accuracy (Table S1). Grain size distribution was analyzed with a particle counter model Mastersizer-2000 at the R + D Services of the University of Huelva using Na-hexametaphosphate as a dispersing agent. Samples were examined by Field Emission Scanning Electron Microscope (FESEM) JEOL JSM-IT500-HR) with an OXFORD X-Max 150 X-ray detector (detecting from B to U). An acceleration potential of 15 kV was applied and a sensor current at 50 % of the equipment capacity (PC50).

3.5. Data treatment

A Principal Component Analysis (PCA) was performed on data (i.e., sediments, DGTs, and chemical extractions) using XLSTAT Basic software to evaluate statistical relationships between multivariate datasets, with the aim of determining the REE and Y partitioning among different environmental compartments (i.e., sediments, DGTs, ion-exchangeable, acid-extractable and carbonate-associated sediment fractions). The statistical relationship between variables in PCA is expressed through their covariance or correlation, in such a way that depending on how much each original variable contributes to a principal component and the correlation between variables we can identify relationships between them. Previously, a normality test (Shapiro-Wilk) was performed on samples. As most variables were non-normally distributed, the Spearman's correlation coefficient was used to determine significant relationships ($\alpha = 0.05$) between data (Davis, 2002). The North American Shale Composite (NASC) values were applied to normalise REE concentrations (Taylor and McLennan, 1985).

4. Results and discussion

4.1. Sediment characterization

Table 1 shows the chemical composition and grain size distribution of estuarine sediments studied, which are mainly characterized by exhibiting silty loam textures with average silt contents of 59.6 %, and lower contents in sands (35.6 %) and clays (4.8 %). However, the estuary outermost sampling point (OS5) exhibited a sandy loam texture with sand contents ranging from 40 to 68 % due to the higher influence of coastal dynamics. The sediments are characterized by their high metal content, with average Fe_2O_3 concentrations of 9.0 % (interquartile range (IR) of 8.5–9.3 %) and maximum of 18 % at the bottom (12–15 cm) of OS2 (Table 1). The average content of Al_2O_3 was 6.4 % (IR of 4.9–7.7 %), with the maximum (15 %) observed in OS1 surface sediments (0–3

Table 1
Chemical composition and grain size distribution of estuarine sediments studied. Clays (<2 μm), silts (2–50 μm) and sands (50–2000 μm).

	Clay	Silt	Sand	Al_2O_3	S_2O_3	K_2O	Na_2O	MgO	CaO	MnO_2	Fe_2O_3	P_2O_5	TiO_2	La	Ce	Pr	Nd	Sm	Eu	Gd	Tb	Dy	Ho	Er	Tm	Yb	Lu	∑REE	Y
	%													mg kg-1															
OS1																													
0–3 cm	4.1	63	33	15	2.6	2.2	4.9	1.9	0.86	0.08	15	0.61	0.79	24	49	6.1	26	6.9	1.5	6.4	0.93	6.1	1.1	3.2	0.44	3.0	0.43	**135**	**26**
3–6 cm	4.1	57	39	7.2	1.7	1.2	3.4	0.88	0.47	0.04	10	0.30	0.44	8.6	21	2.5	11	2.7	0.57	2.7	0.40	2.5	0.47	1.4	0.20	1.4	0.20	56	11
6–9 cm	4.8	65	30	6.3	3.4	1.3	4.0	0.85	0.43	0.04	9.8	0.44	0.53	4.1	10	1.7	7.8	2.2	0.49	2.6	0.41	2.6	0.50	1.5	0.21	1.4	0.21	36	8.7
9–12 cm	5.2	73	22	9.0	1.9	1.6	3.5	0.87	0.47	0.04	9.1	0.33	0.58	10	25	3.0	13	3.1	0.69	3.1	0.46	2.8	0.54	1.6	0.23	1.6	0.24	66	12
12–15 cm	5.6	72	23	7.3	1.8	1.8	2.7	0.74	0.39	0.04	9.7	0.32	0.70	8.2	18	2.3	9.3	2.1	0.47	2.1	0.31	2.0	0.38	1.2	0.17	1.2	0.19	48	8.2
OS2																													
0–3 cm	3.3	63	33	7.6	2.7	1.1	3.8	0.93	0.39	0.04	7.3	0.53	0.39	13	28	4.4	20	5.2	1.1	5.3	0.77	4.6	0.86	2.4	0.34	2.3	0.32	89	19
3–6 cm	3.8	60	36	5.3	1.8	1.1	2.8	0.60	0.23	0.10	8.7	0.51	0.51	3.2	8	1.2	5.7	1.6	0.38	1.9	0.30	2.0	0.39	1.2	0.18	1.2	0.18	27	7.1
6–9 cm	7.4	74	19	4.9	0.73	1.4	2.1	0.33	0.28	0.37	8.5	0.28	0.68	4.6	14	1.3	6.1	1.4	0.31	1.4	0.22	1.4	0.27	0.84	0.13	0.90	0.13	33	4.8
9–12 cm	4.5	55	40	6.4	0.84	1.4	2.3	0.62	0.35	0.21	11	1.5	0.64	8.5	19	2.6	11	2.7	0.60	2.6	0.39	2.3	0.45	1.4	0.19	1.3	0.20	53	10
12–15 cm	5.6	63	31	7.9	1.2	1.2	2.4	0.93	0.65	0.11	18	3.0	0.45	24	49	7.6	34	8.0	1.7	7.3	0.99	5.8	1.1	3.0	0.41	2.7	0.38	**146**	26
OS3																													
0–3 cm	2.6	46	52	8.8	3.0	1.9	2.9	1.6	1.3	0.06	8.0	0.51	0.75	22	46	5.9	25	5.5	1.2	5.2	0.72	4.3	0.83	2.5	0.33	2.3	0.34	122	22
3–6 cm	5.7	71	23	5.8	3.0	1.4	2.5	0.95	0.90	0.07	9.2	0.73	0.73	8.5	22	2.6	12	2.9	0.66	3.1	0.46	2.9	0.56	1.7	0.23	1.6	0.23	59	12
6–9 cm	7.6	78	15	8.0	2.9	1.8	2.1	1.4	0.97	0.06	9.4	0.81	0.68	15	28	4.2	18	4.1	0.91	4.2	0.61	3.8	0.73	2.2	0.30	2.1	0.30	85	18
9–12 cm	7.3	67	26	6.0	3.1	1.4	1.8	0.84	1.7	0.09	9.3	0.98	0.64	14	33	3.8	16	3.8	0.86	4.0	0.56	3.5	0.69	2.0	0.28	1.9	0.27	85	18
12–15 cm	5.9	61	33	6.2	5.7	1.6	1.8	0.92	1.4	0.09	8.9	0.76	0.67	14	30	3.6	16	3.5	0.81	3.7	0.52	3.3	0.66	2.0	0.28	1.9	0.27	81	17
OS4																													
0–3 cm	4.5	66	30	10.0	2.2	1.7	4.3	1.7	2.0	0.07	9.5	0.79	0.66	17	40	4.5	19	4.5	1.0	4.5	0.66	4.1	0.79	2.4	0.33	2.3	0.32	101	19
3–6 cm	5.4	73	21	7.0	2.2	1.6	3.5	1.3	1.1	0.08	10	0.71	0.71	12	29	3.3	14	3.4	0.75	3.4	0.48	3.0	0.59	1.8	0.25	1.7	0.24	74	13
6–9 cm	7.6	80	12	3.9	2.0	1.5	2.7	0.83	0.68	0.07	10	0.72	0.71	6.5	13	2.0	8.7	2.1	0.47	2.2	0.32	2.0	0.39	1.2	0.16	1.1	0.16	40	8.8
9–12 cm	3.4	48	49	7.7	2.0	1.7	2.6	1.2	0.76	0.07	10	0.82	0.71	11	26	3.1	13	2.9	0.64	2.9	0.42	2.7	0.52	1.6	0.22	1.6	0.22	66	12
12–15 cm	4.5	56	40	6.8	2.4	1.6	2.7	1.2	0.78	0.07	11	0.82	0.71	10	22	2.6	11	2.5	0.56	2.6	0.37	2.3	0.48	1.4	0.20	1.4	0.21	57	11
OS5																													
0–3 cm	2.9	37	60	3.6	0.21	1.1	1.2	0.47	2.0	0.04	2.4	0.19	0.37	8.1	17	2.0	8.3	1.7	0.43	1.7	0.23	1.4	0.26	0.76	0.10	0.71	0.10	43	7.4
3–6 cm	3.5	42	55	2.9	0.04	1.0	0.82	0.31	1.5	0.02	1.7	0.12	0.26	9.2	21	2.2	9.1	1.9	0.39	1.7	0.22	1.3	0.23	0.64	0.08	0.57	0.08	48	6.6
6–9 cm	4.7	55	40	2.4	0.07	0.89	0.69	0.25	1.2	0.02	1.4	0.08	0.21	4.8	10	1.2	4.9	1.1	0.29	1.1	0.14	0.8	0.16	0.45	0.06	0.41	0.06	25	4.5
9–12 cm	3.1	35	61	2.8	0.36	1.0	0.92	0.35	1.4	0.03	2.4	0.11	0.32	6.5	16	1.8	7.3	1.7	0.40	1.7	0.22	1.3	0.25	0.75	0.10	0.69	0.10	39	7.1
12–15 cm	2.6	30	68	2.5	0.25	0.80	0.79	0.30	1.7	0.02	1.5	0.07	0.14	6.3	14	1.6	6.8	1.4	0.33	1.3	0.16	0.9	0.17	0.51	0.07	0.46	0.07	34	5.2

cm). Regarding S_2O_3, the average content in sediment was of 1.9 %, with maximum value of 5.7 % at the bottom of OS3 (12–15 cm), while the average content of P_2O_5 was of 0.64 %, reaching the maximum concentrations in the deepest layers of OS2 (up to 3 %; Table 1). Concerning REE and Y, their average content in sediments was of 66 and 13 mg kg^{-1}, respectively. Unlike major components, where slight differences were observed (Table 1), REE and Y concentrations exhibited a great variability, with IR of 40–85 mg kg^{-1} and 7.4–18 mg kg^{-1}, respectively. This may be related to the depositional variability of REY-carrier minerals in the different sediment layers. A general REE and Y enrichment in surface sediments (0–3 cm) is observed, with concentrations above 100 mg $kg^{-1}$and 19 mg kg^{-1}, respectively, in OS1, OS3 and OS4. The only exception was recorded in OS2, where the highest concentrations of REE and Y were observed in depth (12–15 cm; 146 and 26 mg kg^{-1} of REE and Y, respectively), coinciding with the highest contents in P_2O_5. Among REE, the maximum contents were observed for Ce, La, and Nd, which accounted for 61–81 % of total REE. The examination of samples by FESEM (Fig. S2) indicates a mineralogical composition with predominance of quartz and phyllosilicates coated by Fe sulfides and oxides (Fig. SM1, OS2 (0–3)), the latter especially found in the shallower layers. The sulfides observed exhibit a different morphology with, on one hand framboids related to sulfate-reduction processes in the sediments, and, in the other hand angular grains of detrital origin. The presence of phosphates (i.e., monazite (La,Ce(PO_4)), apatite ($Ca_5(PO_4)_3$) and vivianite ($Fe_3(PO_4)_2{\cdot}8H_2O$)), barite ($BaSO_4$) and halite (NaCl) was also identified in some samples, especially in OS2 in the case of phosphates (Fig. S2, OS2 (6–9)).

The PCA performed to determine the geochemical factors controlling the distribution of REE and Y in the estuarine sediments showed a high correlation with Al and Mg (Fig. 1A), and lower with Fe, P, S and Mn, suggesting that REY could be associated to Mg-rich aluminosilicates. However, the composition of estuarine sediments is strongly affected by the nature of elements load transported by rivers. In the case of the Odiel River, deeply affected by AMD, the REY behave conservatively until reaching circumneutral pH values, when REY are scavenged by basaluminite ($Al_4(OH)_{10}SO_4$) precipitation (Lozano et al., 2020b). However, not only the Al-precipitation by acidic water neutralization but also the transport and sedimentation of this element, abundantly found in the particulate matter and sediments of the Odiel River (Pérez-López et al., 2023; Sánchez-España et al., 2005) would explain the high concentrations of REY observed in the fluvial-dominated sediments. The proximity of Fe, S, and P to REY (Fig. 1A) would also suggest their association to Fe oxyhydroxisulfates and phosphates. For instance, the occurrence of phosphates such as monazite has been identified by FESEM in some sediment layers (Fig. S2), especially at the bottom of OS2. In the case of Fe oxyhydroxisulfates, REY can also be effectively sorbed onto schwertmannite ($Fe_8O_8(OH)_6(SO_4)$) at pH values from 4.5 to 6.5 (Lozano et al., 2020a), commonly reached in the upper part of the estuary, when acidic waters mix with seawater (Pérez-López et al., 2023). This neo-formed mineral is also abundantly transported by the Odiel River, especially during flood events (Cánovas et al., 2012; Sánchez-España et al., 2005). As a result of these neutralizing geochemical processes and particulate matter transport, the studied sediments are enriched in Al- and REY as well as Fe.

REE are considered emerging aquatic trace pollutants and studies have revealed significant variability in REE concentration across estuaries, with diverse average total concentrations worldwide, for example 195 μg g^{-1} from 191 sediment samples at the Yellow River estuary (Song et al., 2025), average content of 178 μg g^{-1} in tidal flat sediments from Qidong Cape, Yangtze River estuary (Zhang et al., 2024), REEs and Y concentration from 5.94 to 337 mg kg^{-1} from 12 estuaries along the Atlantic Coast of Brasil (Novais et al., 2024), and from 17 to 522 mg kg^{-1} along the Egyptian Mediterranean coastal areas (Badawy et al., 2022). REE have been used as tracers of geochemical and anthropogenic processes across diverse environments. However, most recent studies evaluating REE in estuarine/coastal environments have been based in determination of concentrations, distribution pattern and main sources in correlation with particle size distribution, Fe, Mn, and Al concentration as well as organic carbon (OC) (Badawy et al., 2022; Novais et al., 2024; Song et al., 2025; Zhang et al., 2024). Since there is still little

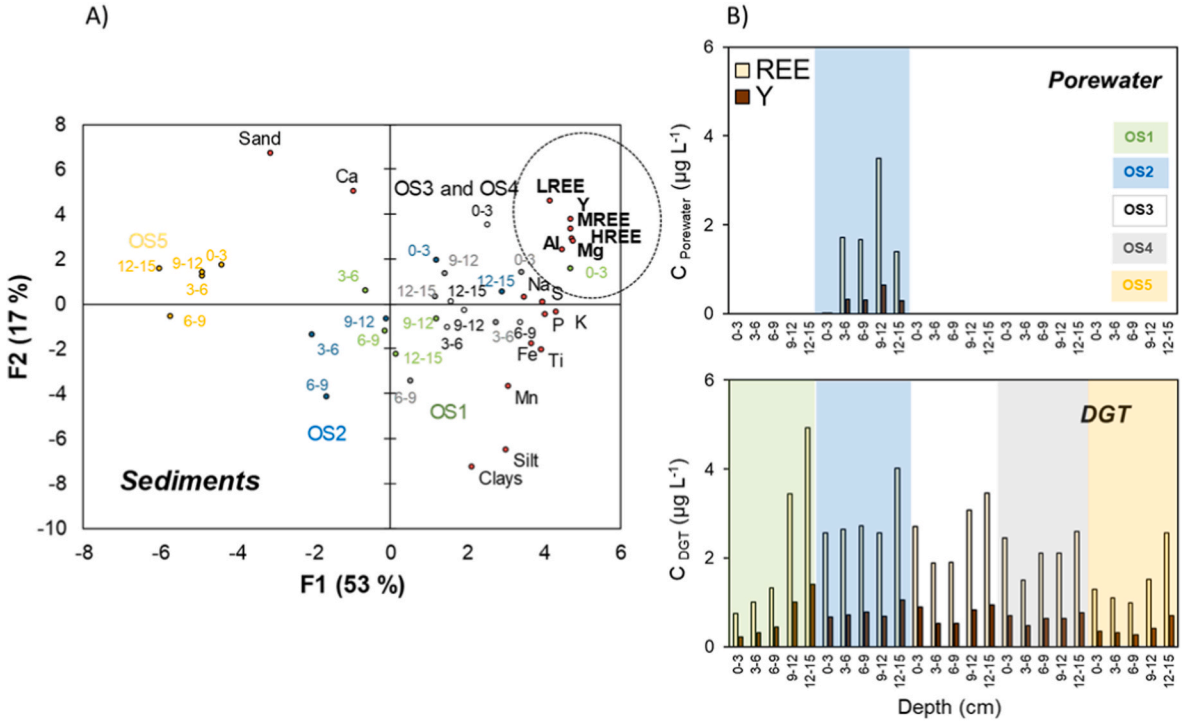

Fig. 1. A) Principal Component Analysis (PCA) of results obtained in bulk sediment composition, B) REE and Y concentration (yellow and brown bars, respectively) in sediment porewater and in diffusive gradient in thin film (DGT) in the sampling points (concentrations in porewater were below the analytical detection limit for most samples). (For interpretation of the references to color in this figure legend, the reader is referred to the Web version of this article.)

information on the presence of REE in coastal systems, such insights are key for evaluating the risks of REE build up and to shape future management and remediation efforts in these ecological relevant systems.

4.2. Metal distribution in porewater and DGTs

Sediments porewater are characterized by high Fe concentration, with the highest value observed in OS1 (from 2269 to 5826 mg kg^{-1}), followed by OS3 and OS4 (from 56 to 506 mg L^{-1} at OS3, and from 35 to 180 mg L^{-1}; Fig. S3). The lowest Fe concentrations were observed in OS2 (from 0.1 to 181 mg kg^{-1}). These high Fe concentrations in porewater may be related to Fe(III)-reduction processes under sediment reducing conditions. Thus, the Fe oxides and oxyhydroxysulfates transported by the river or precipitated by seawater neutralization are settled and buried in the sediment, where are microbiologically dissolved upon reducing conditions. The dissolved ferrous (Fe^{2+}) and sulfide (S^{2-}) leads to the formation of Fe monosulfides and pyrite, which is the final sink of both elements in the reducing sediment subsurface (Kraal et al., 2013), as observed by FESEM images (e.g., OS3 (9–12 cm); Fig. S2). A similar tendency was observed for Mn, with the highest values for OS1 (338–471 mg L^{-1}) and the lowest reached for OS2 (from 25 to 28 mg L^{-1}), except in the top layer, where the Mn concentration (423 mg L^{-1}) was higher than those recorded in the OS3 and OS4 profiles (Fig. S3). Regarding REE and Y, their concentrations in porewater were close to or below the detection limit of the equipment in most samples, except in OS2, where ranged from 0.71 to 3.5 μg L^{-1} and 0.12–0.65 μg L^{-1}, respectively (Fig. 1B), with maximum values found at 9 cm depth (Fig. 1B and S3).

Unlike in porewaters, where concentrations were not detected in most samples, REE and Y were quantified in DGTs (Fig. 1B), highlighting the suitability of these devices to monitor trace pollutants at low concentrations in estuarine sediments. REE concentrations in DGT ranged from 0.75 to 4.9 μg L^{-1}, lower than those reported by Gu et al. (2020) in laboratory experiment, where there were found DGT-labile REE concentrations ranging from 7.0 to 16 μg L^{-1} in intertidal surface sediments of the Pearl River estuary. The sediments from the Daya Bay, a shallow semi-enclosed, mountain-drowned valley bay in the north of the South China Sea, also reported REE concentration ranging from 5.67 to 8.41 μg L^{-1}, still slightly higher than those observed in this study (Gu et al., 2022). Similarly, sediments from the Songhua River system (the third-largest river in China) have been reported to have REE concentration between 2.07 and 8.76 μg L^{-1} (Lu et al., 2022). A spatial trend in REE and Y absorption by DGT was observed, with higher concentration observed in the sites with greater fluvial influence (Fig. 1B), and decreasing values towards the outer part of the estuary due to lower dissolved concentration in the marine domain. Further, increasing values were observed with depth, with maximum REE concentrations recorded at the bottom sediments (e.g., 4.9 μg L^{-1}at OS1, 4.0 μg L^{-1} at OS2, or 3.4 μg L^{-1} at OS3). Although the highest values were recorded in the deeper layers of OS1 (3.4–4.9 μg L^{-1} of REE and 1.0–1.4 μg L^{-1} of Y, below 9 cm: Fig. 1B), the average values ranged from 2.9 μg L^{-1} of REE and 0.77 μg L^{-1} of Y at OS2 to 1.5 μg L^{-1} of REE and 0.41 μg L^{-1} of Y at OS5.

The PCA performed on DGT results (Fig. 2) indicates the proximity of REE and Y to Al, located on the positive side of the first component (42 % of variance), which seems to confirm the suggested association of REY with Al. On the other hand, Fe and Mn appeared close each other on the negative side of this component. Samples from OS2, which exhibited the highest average of REE and Y, are located closer among them and separated from the rest of samples. The increase in concentrations with

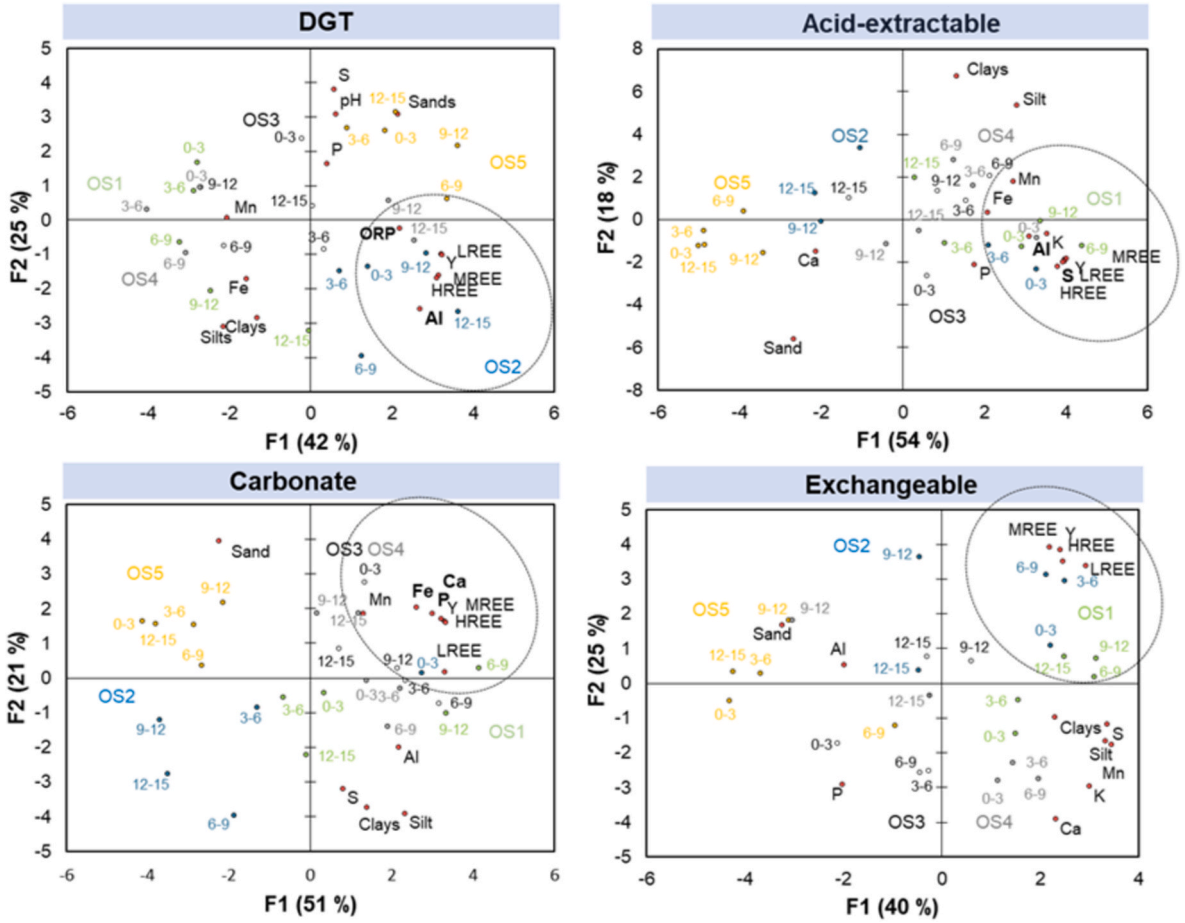

Fig. 2. Principal Component Analysis (PCA) performed on DGT, acid-extractable, carbonate and exchangeable fraction results.

depth is also reflected in the PCA, with the deeper samples (9–12 and 12–15 cm) located nearby this group of elements. This is especially evident in OS1, whose samples are aligned from the negative to the positive side of the first component, getting closer to REE, Y and Al (Fig. 2). This increasing REY concentration with sediment depth might be explained by sulfate reductive biodissolution processes under suboxic conditions (Kerl et al., 2023), which may have led to increasing Fe^{2+} and labile species of REY being diffused by the chelex resin.

4.3. Lability of REE and Y: comparison with sequential extraction schemes

With some variations, first fractions from the conventional sequential extraction approach represent the more mobile elements, which include acid soluble-extractable and exchangeable – carbonate included. Therefore, to know the labile fraction of REY, different extractions commonly applied in sequential extraction schemes were performed (i.e. acid-extractable, ion-exchangeable, and associated to carbonate fractions). In the case of the ion-exchangeable fraction, an electrolyte ($MgCl_2$) at pH 7 is used to avoid oxide and carbonate solubilization and to prevent oxyhydroxide precipitation (Ianni and Ruggieri, 2002). The carbonate fraction is commonly obtained by the addition of a buffer acetic acid-sodium acetate (pH 5), while the acid-extractable phase is determined after the addition of an acid acetic solution. In the case of the carbonate-fraction, some authors report that the extractant does not dissolve all the carbonates, neither attack carbonate selectively, but dissolve labile metals bound to organic matter (Rauret, 1998). Fig. 3 and S4 shows the extraction of REE and Y, correspondingly, in sediments using the different leaching solutions. A minor fraction of total REE and Y (maximum values of 1.1 % and 1.7 %, respectively) was contained in the ion-exchangeable fraction. The extraction was noticeably higher in the fluvial domains of the estuary (i.e., OS1 and OS2; average values of 0.14–0.49 % and 0.34–0.72 % for REE and Y, respectively) than in the seawater domain (OS3, OS4, OS5; below 0.07 and 0.17 %). The PCA obtained for the ion-exchangeable fraction evidences this tendency (Fig. 2), with samples from OS1 and OS2 near to REE and Y. In the case of the carbonate-associated and acid-extractable fractions, a high variability was observed, with values ranging from 3.7 to 74 % for REE and 6.4–94 % for Y in the acid-extractable fraction and from 1.0 to 71 % for REE and 2.0–95 % for Y in the carbonate-associated fraction. Higher acid-extractable values were observed in the fluvial domain (average values of 22–31 % of REE) than in the seawater domain (17–18 %), similar to the ion-exchangeable fraction. However, in the case of the carbonate-associated fraction, the inverse tendency is observed despite recording the highest value in OS1 (6–9 cm) for both REE and Y, with higher extraction values recorded in the outer part of the estuary (average of 27–32 %). This different trend may be related to the sediment mineralogy and the capacity of leaching solutions to dissolve the minerals hosting REE and Y, that is carbonates in the outermost estuary zone. As can be seen in the PCA (Fig. 2), REE and Y appears to be preferentially associated to Al and S in the acid extractable fraction, while in the carbonate-associated fraction these elements seem to be related to Fe, Ca and P. Therefore, the abundance of these minerals along the sediment profile would control the release of these elements during the sequential extractions performed.

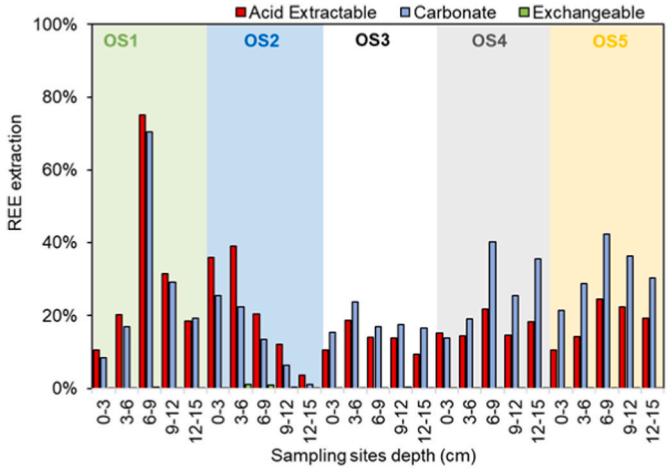

Fig. 3. Rare Earth Elements (REE) extraction in the geochemical fractions, i.e., acid (red bars), carbonate (blue bars), and exchangeable (green bars). The color shading area indicates the different sampling sites (OS1 to OS5). (For interpretation of the references to color in this figure legend, the reader is referred to the Web version of this article.)

The concentration of REE and Y accumulated in DGTs were compared to those contained in the other fractions (i.e., porewater, acid-extractable, carbonate-associated, and ion-exchangeable) (Fig. 4). No relationship between the REE concentration in DGT and pore waters was found, neither with any labile fraction (only represented with respect to acid-extractable in Fig. 4). The only relevant correlation ($R^2 = 0.77$) was observed for REE concentration between the acid-extractable and carbonate fractions. Both solutions (i.e., 0.11 M acetic acid and buffered-sodium acetate) appears to have a similar extraction capacity, but dissolving different minerals according to the performed PCA (i.e., Al oxyhydroxysulfates in the case of the acetic acid, and Fe-Ca phosphate in the case of the buffered-sodium acetate solution). A similar trend is observed for Y, with no apparent relationship between its concentration in DGT and those in pore waters and extractions (Fig. S5). It worth noting that in the case of pore waters, there are only available data from OS2, which preclude drawing any robust conclusion.

4.4. A recent study using the sequential extraction approach to evaluate the potential mobility of trace metallic elements from sediment of the Ria of Huelva estimates between 13 and 18 % release of the total element concentrated in the sediments, with a similar distribution among different pH (Lecomte et al., 2025). Even though some elements such as Co, Cu, or As have shown relatively high release in the fraction 1 (water soluble), REE have shown release below 30 % for sediments at the pH > 5. These are in line with our results, as it was observed low concentration of REE in the porewater as well as in the ion exchangeable fraction, which represent the weakly adsorbed fractions. It implies that REE elements in these sediments are mainly linked to the carbonate and poorly ordered Fe^{3+}-hydroxides and oxyhydroxysulfates. According with these results, DGT passive samplers would be able to incorporate REY from the less mobile fraction, i.e, acid extractable and carbonate-bound fraction as well as from the reducible and oxidisable fractions. **REE fractionation processes in estuarine sediments.**

Fig. 5 shows the NASC-normalized patterns of sediments, pore waters, DGTs, and extractions performed to sediment samples. Sediments are characterized by a MREE enrichment (HREE > LREE), with a slightly depletion of LREE with respect to MREE and HREE. Previous studies have reported the existence of REE fractionation processes in estuarine systems (Lawrence and Kamber, 2006). Thus, during estuarine mixing of river waters rich in inorganic and organic colloids with seawater, LREE may be preferentially partitioned onto these colloids while HREE remain dissolved due to stronger complexation to ligands. However, the acidic nature of the Odiel river waters in this estuary alters this partitioning pattern (Cánovas et al., 2020b), showing the opposite tendency, with a LREE depletion in sediments, which has been previously reported (Lecomte et al., 2017; López-González et al., 2012). This is attributed to the preferential removal of MREE and HREE from the aqueous phase and their accumulation in sediments during the neutralization of acidity transported by the rivers. Once this neutralization is complete, the sediments in the seawater domain possess a HREE depleted pattern with slight Ce anomaly, which is common in marine conditions (Lawrence and Kamber, 2006). As can be seen in Fig. 5, the sediments located within the mixing zone (OS1-OS4) exhibited a LREE depleted NASC-pattern while that more influenced by seawater (OS5) displays a

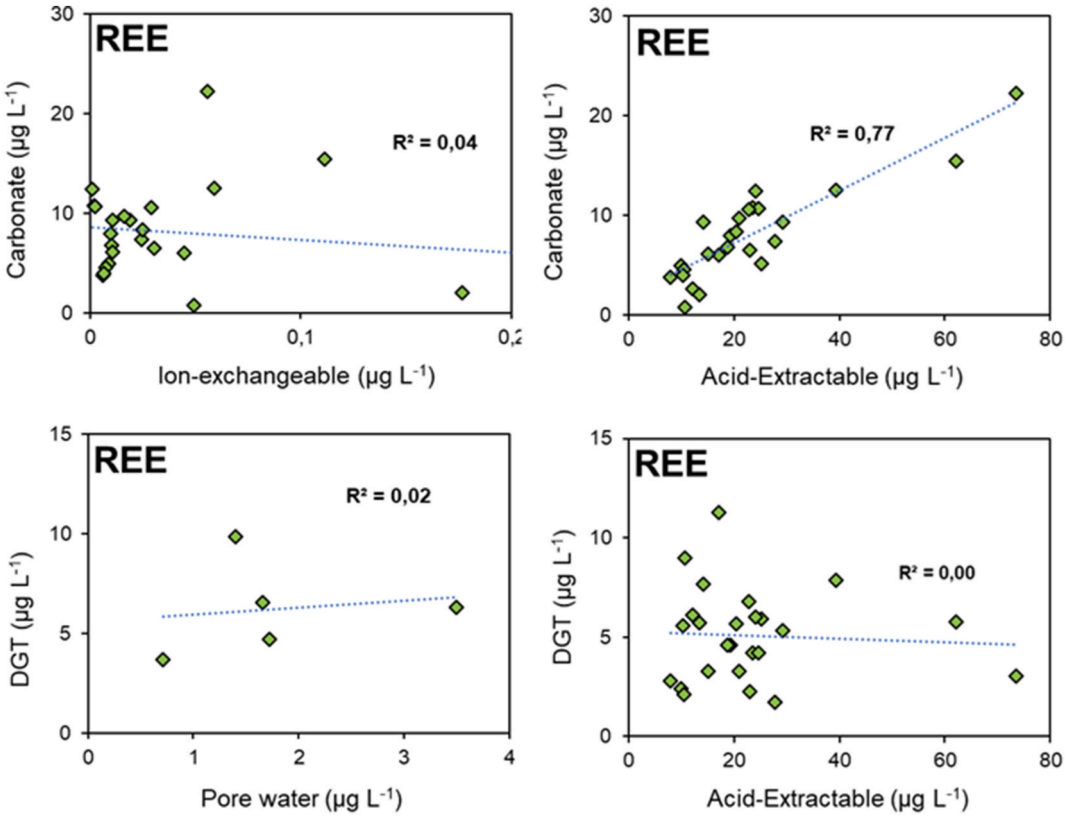

Fig. 4. Relationship between REE concentrations in porewater and labile fractions (i.e., DGT, carbonate, ion-exchangeable and acid-extractable).

pattern typical of marine sediments, with a HREE depleted pattern. This is confirmed by the NASC-normalized pattern observed in porewater results, with an enrichment in LREE with respect to MREE and HREE (LREE > MREE > HREE; Fig. 5), although in this case REE were only detected in OS2.

The NASC-normalized patterns of sediments may reflect the chemical composition of particulate matter transported by the river especially that precipitated during acidic waters neutralization in the mixing zone (Lecomte et al., 2017; Lecomte et al., 2025). These authors reported a preferential accumulation in the residual fraction, with values ranging from 60 to 80 % of total REE, with lower values for the easily soluble, exchangeable, and associated to poorly ordered Fe mineral fractions. As can be seen, the associated to carbonate and acid-extractable fractions seems to have inherited the REE NASC-normalized pattern of the sediment, characterized by a strong enrichment in MREE (Fig. 5). However, some differences in patterns can be noted. On the one hand, the acid-extractable fraction exhibited to some extent higher enrichment in LREE over HREE while the opposite is observed in the fraction associated to carbonates (HREE > LREE). The acid-extractable fraction may include those minerals easily soluble under mild acidic conditions. The relationship observed between REE, Al and S (and to a lesser extent with Fe) in the PCA (Fig. 2) seems to indicate that the main contributor minerals in this fraction are Al hydroxysulfates. In turn, in the case of the carbonate associated fraction, the occurrence of REE seems to be related to Fe and Ca phosphates and carbonates. The selectivity of reagents used for both fractions (acid-extractable and associated to carbonate) is not clear, and sometimes are used indistinctly for the same purpose (Rauret, 1998). This is supported by the correlation (R^2 = 0.74–0.77; Fig. 5 and SM4) observed between REE and Y concentrations in both extractions. In the case of the ion-exchangeable fraction, a nearly flat REE-NASC pattern is observed (Fig. 5). Lecomte et al. (2017) attributed the presence of REE in the ion-exchangeable fraction to desorption processes from poorly-ordered Fe minerals, discarding the clays and organic matter as carrier phases since adsorption at low pH values is not significant. This is consistent with PCA results, where REE and Y are located together but far away from other elements (Fe was below detection limit in this fraction). Regarding the NASC-normalized pattern of DGTs, a MREE-enrichment is observed (Fig. 5) with respect to LREE and HREE. The DGTs quantify the labile species during the deployment, which depends on the concentration at the interface between the device surface and the sediment, being usually similar to the concentration in pore-waters. Therefore, a similar REE NASC-normalized pattern to that of porewater would be expected. Conversely, the patterns observed in DGTs seems to be more influenced by those observed in sediments (and the sequential acid- and carbonate extractions), which suggest the passing of colloids contained in the sediments through the membranes of the DGTs. In this sense, the closeness of REY to Al in the PCA for DGTs (Fig. 2) suggests the absorption of Al colloids by DGTs. This fact would have notable implications for the validation of these devices for monitoring REE and Y exposure in estuarine sediments. Unlike the general belief of the similarities of DGT metal concentrations with porewater concentrations; these devices can also absorb and concentrate nanoparticles and colloids of size lower than 0.45 µm.

Fractionation studies have shown that at coastal areas a right-dipping negative slope pattern, with relatively frequent enrichment in the LREE (La, Ce, Pr, and Nd)) over HREE (Er, Tm, Yb, and Lu) is often observed, explained by the preferential scavenging of LREE by colloids, and adsorption and/or incorporation in clay minerals formed during chemical weathering, whereas HREE depletion is related to their complexation with soluble carbonate fractions and dissolved organic and inorganic ligands (de Freitas et al., 2021; Novais et al., 2024). In addition, normalized patterns indicate natural processes predominantly controlling REE distributions in estuarine environments over anthropogenic sources (e.g., Novais et al., 2024; Song et al., 2025) as geological signatures strongly influencing REE concentrations and fractionation. Moreover, the fresh- and salt-water interface in estuaries may impact

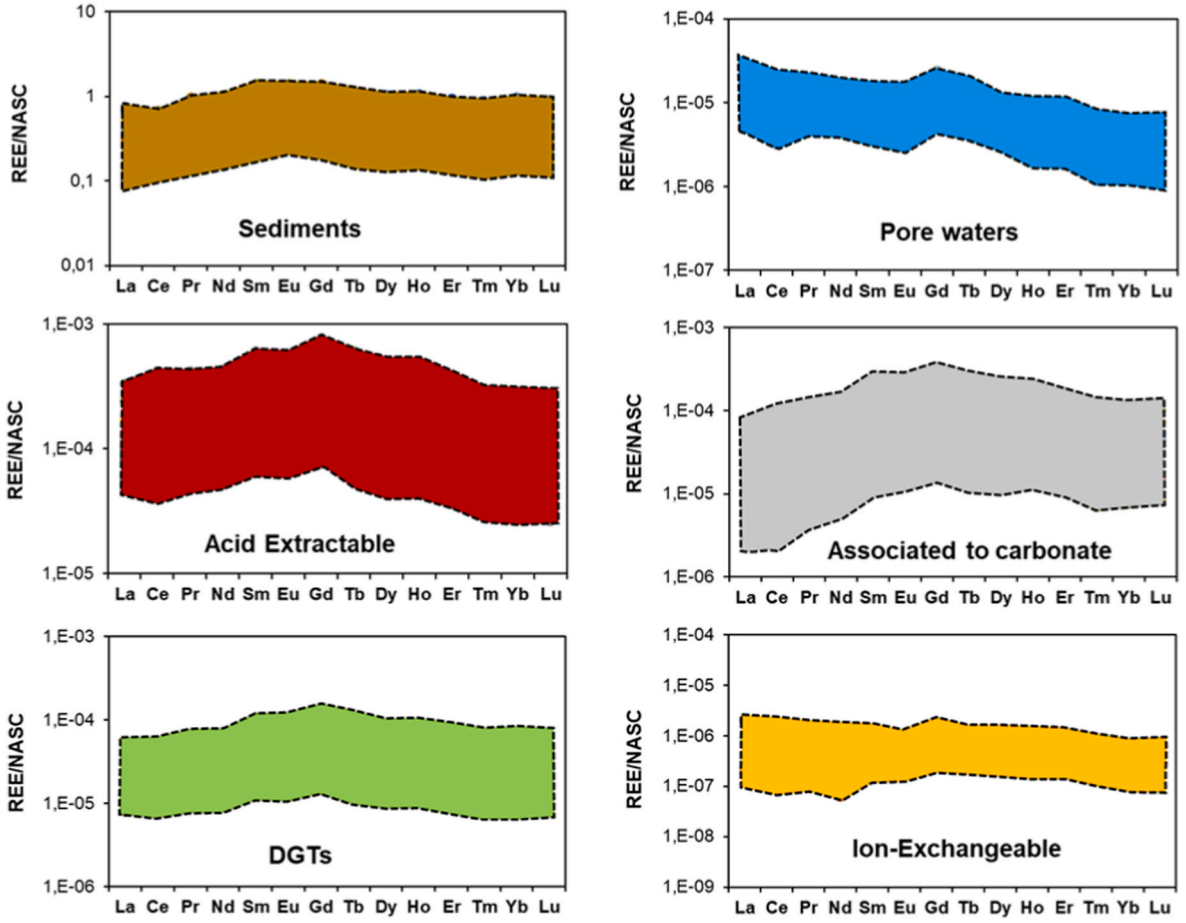

Fig. 5. NASC normalized patterns of REE in sediments, porewaters, DGT and geochemical fractions.

metal speciation, leading to changes in bioavailability and bioaccumulation in aquatic organism, for example in clams (Desjardins et al., 2025). However, the association between DGTs concentrations and exposed organisms bioaccumulation is not such evident yet (Feng et al., 2022; Gu et al., 2020; Gu et al., 2023; Xu et al., 2024), which in the case of REY might be explained because these elements are not commonly associated with the most mobile fraction in estuarine sediments. However, such correlation between DGT concentration and available fractions has been proved for other potentially toxic elements as Cu, Zn or Cd (Feng et al., 2022; Galgani et al., 2025).

4.4. Environmental implications

Although the use of DGTs is still emerging, they represent a promising method for determining the presence and concentration of REEs in areas where sampling is challenging. For instance, DGTs could be applied in preliminary investigations of deep-sea Fe–Mn polymetallic nodules (Hikov et al., 2025), where REE occurrence and the potential for exploiting these deposits as critical raw material resources have been extensively studied. Our results show no correlation between dissolved pore water concentrations and DGT-labile fractions. DGTs selectively accumulate truly dissolved species (free ions and weak complexes), providing more accurate exposure estimates. Their in situ, time-integrated nature and sensitivity make them effective for assessing trace metal risks. The comparison of DGT concentrations with those obtained applying leaching solutions commonly used to determine labile fractions in sediments (i.e., exchangeable, acid-soluble, carbonate-associated) provided different results, suggesting the application of sequential extractions may be not appropriate to assess toxicity in estuarine and coastal sediments. For all these reasons, REE distribution in estuarine sediments as well as their exposure to benthic organisms should be monitored by DGTs deployment as part as programs assessing their environmental quality status. Originally developed for metals like Pb, Cd, Cu, Zn, Ni, and Co, DGTs also show promise for REY monitoring, though further validation is needed. We support calls for standardized guidelines (e.g., Amouroux et al., 2023; Miège et al., 2015) to integrate DGTs into EU regulatory frameworks such as the Water Framework Directive and the Marine Strategy Framework Directive.

5. Conclusions

The distribution and availability of REE and Y in estuarine sediments strongly affected by mining was studied in solids, pore waters, and labile fractions performed using passive samplers and different sequential extraction to recover labile metals. The studied sediments are characterized by their high metal concentrations, with average concentrations of 9.0 % of Fe_2O_3, 6.4 % of Al_2O_3, 1.9 % of S_2O_3, and 66 and 13 mg kg^{-1} of REE and Y, respectively. REE sources may include Al oxyhydrosulfates (e.g., basaluminite), Fe and REE phosphates, and associations with Fe oxyhydroxysulfates and aluminosilicates. While REE and Y concentrations in porewaters were often below detection limits, DGTs effectively retained them, confirming their utility for monitoring trace pollutants. A spatial trend in REE and Y uptake by DGTs was observed, with higher values at depth and in river-influenced sites.

Ion-exchangeable REE and Y concentrations were low, with higher values in fluvial than marine domains. The carbonate-associated and acid-extractable fractions showed variability, with REE values ranging from 3.7 to 74 % and 1.0–71 %, and Y from 6.4 to 94 % and 2.0–95 %, respectively. PCA indicated REY was linked to Al and S in acid-extractable fractions, and to Fe, Ca, and P in carbonate-associated

ones. No significant correlations were found between DGT concentrations and those from porewaters or other labile fractions.

NASC-normalized patterns allowed tracing the origin of REY retained in DGTs. A MREE-enrichment is observed in DGTs with respect LREE and HREE, which does not coincide with that of porewater (LREE enriched). On the contrary, the patterns observed in DGTs seems to be more influenced by those observed in sediments, which suggest the passing of colloids contained in the sediments through the membranes of the DGTs. This information would have important implications for the validation of these devices for monitoring REE and Y in estuarine sediments. Unlike the general belief of the similarities of DGT metal concentrations with porewater concentrations, these devices seem to absorb nanoparticles and colloids of size lower than 0.45 μm. Another possibility is that DGTs would concentrate these elements up to a measurable concentration, unlike in porewater where the concentration is below the detection limit. Therefore, further research is needed to confirm this possibility.

CRediT authorship contribution statement

María Dolores Basallote: Writing – original draft, Methodology, Investigation, Funding acquisition, Formal analysis, Data curation, Conceptualization. **Aarón Méndez:** Writing – review & editing, Methodology, Investigation, Data curation, Conceptualization. **Rafael León:** Writing – review & editing, Visualization, Validation, Formal analysis. **Manuel Olías:** Writing – review & editing, Methodology, Investigation. **Rémi Freydier:** Writing – review & editing, Validation, Formal analysis. **Rafael Pérez-López:** Writing – review & editing, Visualization, Validation, Investigation. **Carlos Ruiz Cánovas:** Writing – review & editing, Writing – original draft, Visualization, Validation, Supervision, Funding acquisition, Conceptualization.

Declaration of competing interest

The authors declare that they have no known competing financial interests or personal relationships that could have appeared to influence the work reported in this paper.

Acknowledgments

M. D. Basallote thanks the Spanish State Research Agency (AEI) for the RYC2022-035326-I grant funded by MICIU/AEI/10.13039/501100011033 and FSE+. This work was supported by the Spanish Ministry of Science, Innovation and Universities under the research project DYNAMICO (PID2023-151504OB-I00) funded by MICIU/AEI/10.13039/501100011033. This research was also supported by ERA-MIN3 SuMRee project (PCI2024-153500), financed by MICIU/AEI/10.13039/501100011033, and by the European Union NextGeneration EU/PRTR.

Appendix A. Supplementary data

Supplementary data to this article can be found online at https://doi.org/10.1016/j.envpol.2025.127304.

Data availability

Data will be made available on request.

References

Amato, E.D., Simpson, S.L., Jarolimek, C.V., Jolley, D.F., 2014. Diffusive gradients in thin films technique provide robust prediction of metal bioavailability and toxicity in estuarine sediments. Environ. Sci. Technol. 48 (8), 4485–4494.

Amato, E.D., Simpson, S.L., Remaili, T.M., Spadaro, D.A., Jarolimek, C.V., Jolley, D.F., 2016. Assessing the effects of bioturbation on metal bioavailability in contaminated sediments by diffusive gradients in thin films (DGT). Environ. Sci. Technol. 50 (6), 3055–3064.

Amato, E.D., Wadige, C.P.M., Taylor, A.M., Maher, W.A., Simpson, S.L., Jolley, D.F., 2018. Field and laboratory evaluation of DGT for predicting metal bioaccumulation and toxicity in the freshwater bivalve Hyridella australis exposed to contaminated sediments. Environ. Pollut. 243, 862–871.

Amouroux, I., Gonzalez, J.-L., Guesdon, S., Belzunce-Segarra, M.J., Bersuder, P., Bolam, T., Caetano, M., Correia Dos Santos, M., Larreta, J., Lebrun, L., Marras, B., Millán Gabet, V., McHugh, B., Menchaca, I., Menet-Nédélec, F., Montero, N., Perceval, O., Pierre-Duplessix, O., Regan, F., Rodríguez, J.G., Rodrigo Sanz, M., Schintu, M., White, B., Zhang, H., 2023. A new approach to using diffusive gradient in thin-films (DGT) labile concentration for water framework directive chemical status assessment: adaptation of environmental quality standard to DGT for cadmium, nickel and lead. Environ. Sci. Eur. 35 (1), 29. https://doi.org/10.1186/s12302-12023-00733-12304.

Ardelan, M.V., Steinnes, E., Lierhagen, S., Linde, S.O., 2009. Effects of experimental CO2 leakage on solubility and transport of seven trace metals in seawater and sediment. Sci. Total Environ. 407 (24), 6255–6266. https://doi.org/10.1016/j.scitotenv.2009.6209.6004.

Arienzo, M., Ferrara, L., Trifuoggi, M., Toscanesi, M., 2022. Advances in the fate of rare earth elements, REE, in transitional environments: coasts and estuaries. Water 14 (3), 401. https://doi.org/10.3390/w14030401.

Badawy, W., Elsenbawy, A., Dmitriev, A., El Samman, H., Shcheglov, A., El-Gamal, A., Kamel, N.H., Mekewi, M., 2022. Characterization of major and trace elements in coastal sediments along the Egyptian Mediterranean Sea. Mar. Pollut. Bull. 177, 113526.

Basallote, M.D., Borrero-Santiago, A.R., Canovas, C.R., Hammer, K.M., Olsen, A.J., Ardelan, M.V., 2020. Trace metal mobility in sub-seabed sediments by CO2 seepage under high-pressure conditions. Sci. Total Environ. 700, 134761. https://doi.org/10.131016/j.scitotenv.132019.134761, 1347.

Besada, V., Bellas, J., Sánchez-Marín, P., Bernárdez, P., Schultze, F., 2022. Metal and metalloid pollution in shelf sediments from the Gulf of Cádiz (Southwest Spain): long-lasting effects of a historical mining area. Environ. Pollut. 295, 118675. https://doi.org/10.111016/j.envpol.112021.118675, 1186.

Borrego, J., López-González, N., Carro, B., Group, C.G., 2004. Geochemical signature as paleoenvironmental markers in Holocene sediments of the Tinto River estuary (Southwestern Spain). Estuar. Coast Shelf Sci. 61 (4), 631–641. https://doi.org/10.1016/j.ecss.2004.1007.1004.

Brito, P., Prego, R., Mil-Homens, M., Caçador, I., Caetano, M., 2018. Sources and distribution of yttrium and rare earth elements in surface sediments from Tagus estuary, Portugal. Sci. Total Environ. 621, 317–325. https://doi.org/10.1016/j.scitotenv.2017.1011.1245.

Cánovas, C.R., Basallote, M.D., Borrego, P., Millán-Becerro, R., Pérez-López, R., 2020a. Metal partitioning and speciation in a mining-impacted estuary by traditional and passive sampling methods. Sci. Total Environ. 722, 137905. https://doi.org/10.131016/j.scitotenv.132020.137905, 1379.

Cánovas, C.R., Basallote, M.D., Macías, F., 2020b. Distribution and availability of rare earth elements and trace elements in the estuarine waters of the Ría of Huelva (SW Spain). Environ. Pollut. 267, 115506. https://doi.org/10.111016/j.envpol.112020.115506, 1155.

Cánovas, C.R., Basallote, M.D., Macías, F., Olías, M., Pérez-López, R., Ayora, C., Nieto, J. M., 2021. Geochemical behaviour and transport of technology critical metals (TCMs) by the Tinto River (SW Spain) to the Atlantic Ocean. Sci. Total Environ. 764, 143796. https://doi.org/10.141016/j.scitotenv.142020.143796, 1437.

Cánovas, C.R., Macías, F., López, R.P., Nieto, J.M., 2018. Mobility of rare earth elements, yttrium and scandium from a phosphogypsum stack: environmental and economic implications. Sci. Total Environ. 618, 847–857. https://doi.org/10.1016/j.scitotenv.2017.1008.1220.

Cánovas, C.R., Olias, M., Sarmiento, A.M., Nieto, J.M., Galván, L., 2012. Pollutant transport processes in the Odiel River (SW Spain) during rain events. Water Resour. Res. 48 (6). https://doi.org/10.1029/2011WR011041.

Chakhmouradian, A., Wall, F., 2012. Rare earth elements: minerals, mines, magnets (and more). Elements 8, 333–340. https://doi.org/10.2113/gselements.2118.2115.2333.

Cindrić, A.-M., Marcinek, S., Garnier, C., Salaün, P., Cukrov, N., Oursel, B., Lenoble, V., Omanović, D., 2020. Evaluation of diffusive gradients in thin films (DGT) technique for speciation of trace metals in estuarine waters - a multimethodological approach. Sci. Total Environ. 721, 137784. https://doi.org/10.131016/j.scitotenv.132020.137784, 1377.

Davis, J.C., 2002. Statistics and Data Analysis in Geology. Jonh Wiley & Sons, USA.

Davison, W., 2016. Diffusive Gradients in thin-films for Environmental Measurements. Cambridge University Press.

de Freitas, T.O.P., Pedreira, R.M.A., Hatje, V., 2021. Distribution and fractionation of rare earth elements in sediments and mangrove soil profiles across an estuarine gradient. Chemosphere 264, 128431.

Delgado, J., Pérez-López, R., Galván, L., Nieto, J.M., Boski, T., 2012. Enrichment of rare earth elements as environmental tracers of contamination by acid mine drainage in salt marshes: a new perspective. Mar. Pollut. Bull. 64 (9), 1799–1808. https://doi.org/10.1016/j.marpolbul.2012.1706.1001, 17.

Desjardins, K., Ponton, D.E., Bilodeau, F., Rosabal, M., Amyot, M., 2025. Determinants of trace element accumulation in soft-shell clams (Mya arenaria) in Eastern Canada and implications for human consumption. J. Hazard Mater. 493, 138385.

Directive, W.F., 2000. 2000/60/EC Directive 2000/60/EC of the European Parliament and of the Council of 23 October 2000 Establishing a Framework for Community Action in the Feld of Water Policy, 22.12. Ofcial Journal of the European Union L327/1.

Eggert, R.G., 2011. Minerals go critical. Nat. Chem. 3 (9), 688–691. https://doi.org/10.1038/NCHEM.1116.
Feng, W., Wang, Z., Zhu, W., Zheng, F., Zhang, D., Xu, H., 2022. Evaluation of the bioavailability of metals in sediment from the Southern coastal wetland of the qiantang Estuary by using diffusive gradients in thin films technique. J. Ocean Univ. China 21 (2), 375–387.
Galgani, F., Bouchoucha, M., Brach Papa, C., Andral, B., Connes, C., Gonzalez, J.L., Tomasino, C., Paoli, C., Baldi, Y., Chiffoleau, J.F., 2025. Long term changes of associated metal contamination of marine sediments affected by coastal mining of asbestos. Mar. Pollut. Bull. 217, 118093.
Gao, Y., Lesven, L., Gillan, D., Sabbe, K., Billon, G., De Galan, S., Elskens, M., Baeyens, W., Leermakers, M., 2009. Geochemical behavior of trace elements in subtidal marine sediments of the Belgian coast. Mar. Chem. 117 (1), 88–96. https://doi.org/10.1016/j.marchem.2009.1005.1002.
Gao, Y., Zhou, C., Gaulier, C., Bratkic, A., Galceran, J., Puy, J., Zhang, H., Leermakers, M., Baeyens, W., 2019. Labile trace metal concentration measurements in marine environments: from coastal to open ocean areas. TrAC, Trends Anal. Chem. 116, 92–101. https://doi.org/10.1016/j.trac.2019.1004.1027.
Geagea, M.L., Stille, P., Millet, M., Perrone, T., 2007. REE characteristics and Pb, Sr and Nd isotopic compositions of steel plant emissions. Sci. Total Environ. 373 (1), 404–419. https://doi.org/10.1016/j.scitotenv.2006.1011.1011.
Gillmore, M.L., Price, G.A., Golding, L.A., Stauber, J.L., Adams, M.S., Simpson, S.L., Smith, R.E., Jolley, D.F., 2021. The diffusive gradients in thin films technique predicts sediment nickel toxicity to the amphipod Melita plumulosa. Environ. Toxicol. Chem. 40 (5), 1266–1278. https://doi.org/10.1002/etc.4971, 12.
Grantcharova, M.M., Fernández-Caliani, J.C., 2021. Soil acidification, mineral neoformation and heavy metal contamination driven by weathering of sulphide wastes in a Ramsar wetland. Appl. Sci. 12 (1), 249. https://doi.org/10.3390/app12010249.
Gu, Y.-G., Gao, Y.-P., Huang, H.-H., Wu, F.-X., 2020. First attempt to assess ecotoxicological risk of fifteen rare earth elements and their mixtures in sediments with diffusive gradients in thin films. Water Res. 185, 116254. https://doi.org/10.111016/j.watres.112020.116254, 1162.
Gu, Y.-G., Huang, H.-H., Gong, X.-Y., Liao, X.-L., Dai, M., Yang, Y.-F., 2022. Application of diffusive gradients in thin films to determine rare earth elements in surface sediments of Daya Bay, China: occurrence, distribution and ecotoxicological risks. Mar. Pollut. Bull. 181, 113891. https://doi.org/10.111016/j.marpolbul.112022.113891, 1138.
Gu, Y.-G., Wang, Y.-S., Jordan, R.W., Su, H., Jiang, S.-J., 2023. Probabilistic ecotoxicological risk assessment of heavy metal and rare earth element mixtures in aquatic biota using the DGT technique in coastal sediments. Chemosphere 329, 138592.
Hikov, A., Milakovska, Z., Peytcheva, I., Stoyanova, V., Stefanova, E., Abramowski, T., Kadiyski, M., Chavdarova, S., Stavrev, M., Dimitrova, D., 2025. Geochemistry of REE and other critical elements in deep-sea polymetallic nodules from interoceanmetal (IOM) exploration area in eastern part of clarion–clipperton fracture zone, NE Pacific. Minerals 15 (2), 154.
Ianni, C., Ruggieri, N., 2002. Chemistry of Marine Water and Sediments. Springer, pp. 455–468.
IUPAC 2005, Damhus, Ture, Hartshorn, R.M., Hutton, A.T., 2005. Nomenclature of Inorganic Chemistry: IUPAC Recommendations, pp. 25–26.
Kerl, C.F., Basallote, M.D., Käberich, M., Oldani, E., Espejo, N.P.C., Blanco, A.E.C., Cánovas, C.R., Nieto, J.M., Planer-Friedrich, B., 2023. Consequences of sea level rise for high metal (loid) loads in the Ría of Huelva estuary sediments. Sci. Total Environ. 873, 162354. https://doi.org/10.161016/j.scitotenv.162023.162354, 1623.
Kraal, P., Burton, E.D., Bush, R.T., 2013. Iron monosulfide accumulation and pyrite formation in eutrophic estuarine sediments. Geochem. Cosmochim. Acta 122, 75–88. https://doi.org/10.1016/j.gca.2013.1008.1013.
Lawrence, M.G., Kamber, B.S., 2006. The behaviour of the rare earth elements during estuarine mixing—revisited. Mar. Chem. 100 (1–2), 147–161. https://doi.org/10.1016/j.marchem.2005.1011.1007.
Lecomte, K.L., Sarmiento, A., Borrego, J., Nieto, J., 2017. Rare earth elements mobility processes in an AMD-affected estuary: huelva Estuary (SW Spain). Mar. Pollut. Bull. 121 (1–2), 282–291. https://doi.org/10.1016/j.marpolbul.2017.1006.1030.
Lecomte, K.L., Yaciuk, P.A., Sarmiento, A.M., Borrego, J., Nieto, J.M., 2025. Geochemistry of sediment precipitated during acid mine drainage-seawater interaction. Implications for metal mining impacts on estuarine systems. Chem. Geol. 684, 122794.
López-González, N., Borrego, J., Carro, B., Grande, J.A., De la Torre, M., Valente, T., 2012. Rare-earth-element fractionation patterns in estuarine sediments as a consequence of acid mine drainage: a case study in SW Spain. Bol. Geol. Min. 123 (1), 55–56.
López-González, N., Borrego, J., Morales, J., Carro, B., Lozano-Soria, O., 2006. Metal fractionation in oxic sediments of an estuary affected by acid mine drainage (southwestern Spain). Estuar. Coast Shelf Sci. 68 (1–2), 297–304. https://doi.org/10.1016/j.ecss.2006.1001.1020.
Lozano, A., Ayora, C., Fernández-Martínez, A., 2020a. Sorption of rare earth elements on schwertmannite and their mobility in acid mine drainage treatments. Appl. Geochem. 113, 104499. https://doi.org/10.101016/j.apgeochem.102019.104499, 1044.
Lozano, A., Ayora, C., Macías, F., León, R., Gimeno, M.J., Auqué, L., 2020b. Geochemical behavior of rare earth elements in acid drainages: modeling achievements and limitations. J. Geochem. Explor. 216, 106577. https://doi.org/10.101016/j.gexplo.102020.106577, 1065.
Lu, X.-X., Gu, Y.-G., Wang, Z.-H., Liang, R.-Z., Han, Y.-J., Li, H.-S., 2022. Risk on assessment of 15 REEs and mixtures by DGT in Songhua River system sediments of China's largest old industrial base. Environ. Res. 212, 113368. https://doi.org/10.111016/j.envres.112022.113368, 1133.
Marrugo-Madrid, S., Turull, M., Zhang, H., Díez, S., 2021. Diffusive gradients in thin films for the measurement of labile metal species in water and soils: a review. Environ. Chem. Lett. 19 (5), 3761–3788. https://doi.org/10.1007/s10311-10021-01246-10313, 37.
Menegário, A.A., Yabuki, L.N.M., Luko, K.S., Williams, P.N., Blackburn, D.M., 2017. Use of diffusive gradient in thin films for in situ measurements: a review on the progress in chemical fractionation, speciation and bioavailability of metals in waters. Anal. Chim. Acta 983, 54–66. https://doi.org/10.1016/j.aca.2017.1006.1041.
Miège, C., Mazzella, N., Allan, I., Dulio, V., Smedes, F., Tixier, C., Vermeirssen, E., Brant, J., O'Toole, S., Budzinski, H., Ghestem, J.-P., Staub, P.-F., Lardy-Fontan, S., Gonzalez, J.-L., Coquery, M., Vrana, B., 2015. Position paper on passive sampling techniques for the monitoring of contaminants in the aquatic environment – achievements to date and perspectives. Trends Environ. Anal. Chem. 8, 20–26. https://doi.org/10.1016/j.teac.2015.1007.1001.
Neira, P., Romero-Freire, A., Basallote, M.D., Qiu, H., Cobelo-Garcia, A., Canovas, C.R., 2022. Review of the concentration, bioaccumulation, and effects of lanthanides in marine systems. Front. Mar. Sci. 9, 920405. https://www.frontiersin.org/articles/920410.923389/fmars.922022.920405.
Nieto, J.M., Sarmiento, A.M., Olías, M., Canovas, C.R., Riba, I., Kalman, J., Delvalls, T.A., 2007. Acid mine drainage pollution in the Tinto and Odiel rivers (Iberian Pyrite Belt, SW Spain) and bioavailability of the transported metals to the Huelva Estuary. Environ. Int. 33 (4), 445–455.
Novais, F.C., Hatje, V., Hadlich, H.L., Bernardino, A.F., Yogui, G.T., 2024. Rare earth elements and yttrium along eastern Atlantic estuaries. Mar. Chem. 265–266, 104426.
Panther, J.G., Bennett, W.W., Welsh, D.T., Teasdale, P.R., 2014. Simultaneous measurement of trace metal and oxyanion concentrations in water using diffusive gradients in thin films with a Chelex–Metsorb mixed binding layer. Anal. Chem. 86 (1), 427–434. https://doi.org/10.1021/ac402247j.
Pérez-López, R., Millán-Becerro, R., Basallote, M.D., Carrero, S., Parviainen, A., Freydier, R., Macías, F., Cánovas, C.R., 2023. Effects of estuarine water mixing on the mobility of trace elements in acid mine drainage leachates. Mar. Pollut. Bull. 187, 114491. https://doi.org/10.111016/j.marpolbul.112022.114491, 1144.
Philipps, R.R., Xu, X., Bringolf, R.B., Mills, G.L., 2019. Evaluation of the DGT technique for predicting uptake of metal mixtures by fathead minnow (Pimephales promelas) and yellow lampmussel (Lampsilis cariosa). Environ. Toxicol. Chem. 38 (1), 61–70.
Rauret, G., 1998. Extraction procedures for the determination of heavy metals in contaminated soil and sediment. Talanta 46 (3), 449–455. https://doi.org/10.1016/S0039-9140(1097)00406-00402.
Rosado, D., Usero, J., Morillo, J., 2015. Application of a new integrated sediment quality assessment method to Huelva estuary and its littoral of influence (Southwestern Spain). Mar. Pollut. Bull. 98 (1–2), 106–114. https://doi.org/10.1016/j.marpolbul.2015.1007.1008.
Ruiz, F., Vidal, J.R., Cáceres, L.M., Olías, M., González-Regalado, M.L., Campos, J.M., Bermejo, J., Abad, M., Izquierdo, T., Carretero, M.I., 2020. Silver and copper as pollution tracers in Neogene to Holocene estuarine sediments from southwestern Spain. Mar. Pollut. Bul. 150, 110704. https://doi.org/10.111016/j.marpolbul.112019.110704, 1107.
Sainz, A., Grande, J., De la Torre, M., 2004. Characterisation of heavy metal discharge into the Ria of Huelva. Environ. Int. 30 (4), 557–566.
Sánchez-España, J., Pamo, E.L., Santofimia, E., Aduvire, O., Reyes, J., Barettino, D., 2005. Acid mine drainage in the Iberian Pyrite Belt (Odiel river watershed, Huelva, SW Spain): geochemistry, mineralogy and environmental implications. Appl. Geochem. 20 (7), 1320–1356. https://doi.org/10.1016/j.apgeochem.2005.1301.1011.
Song, W., Wu, Z., Yi, W., Wang, S., Zhang, H., Liu, J., 2025. Rare earth elements in the Yellow River estuary, China: composition, distribution, and pollution insights. Mar. Pollut. Bull. 212, 117599.
Taylor, S.R., McLennan, S.M., 1985. The Continental Crust: Its Composition and Evolution 312. Blackwell Scientific, Boston, Mass.
Xu, D., Xiong, H., Wu, Q., Xiao, W., Simpson, S.L., Tan, Q.-G., Chen, R., Xie, M., 2024. Sediment ballet: unveiling the dynamics of metal bioavailability in sediments following resuspension and reequilibration. Environ. Sci. Technol. 58 (51), 22755–22765.
Yuan, Y., Ding, S., Wang, Y., Zhang, L., Ren, M., Zhang, C., 2018. Simultaneous measurement of fifteen rare earth elements using diffusive gradients in thin films. Anal. Chim. Acta 1031, 98–107. https://doi.org/10.1016/j.aca.2018.1005.1067.
Zhang, Y., Zhang, Z., Stephenson, W., Chen, Y., 2024. Geochemical behavior of rare Earth elements in tidal flat sediments from Qidong cape, Yangtze River Estuary: implications for the study of sedimentary environmental change. Land 13 (9), 1425.